ACS Photonics

pubs.acs.org/journal/apchd5

Article

Black Phosphorus Photodetector Enhanced by a Planar Photonic Crystal Cavity

Ruijuan Tian, Linpeng Gu, Yingke Ji, Chen Li, Yuxin Chen, Siqi Hu, Zhiwen Li, Xuetao Gan,* and Jianlin Zhao

Cite This: https://doi.org/10.1021/acsphotonics.1c01168

Read Online

ACCESS | Metrics & More | Article Recommendations | Supporting Information

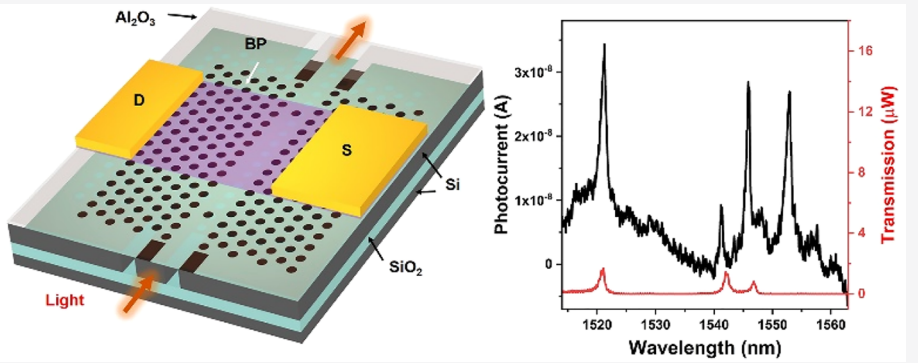

ABSTRACT: We report the integration of a black phosphorus (BP) photodetector on a silicon planar photonic crystal cavity for improving the performance. Benefiting from the cavity-enhanced light−BP interaction, the device has a compact footprint, promising high responsivity, low dark current, and high speed. With an on-resonance excitation, the photodetection is enhanced by 36 times over that obtained with the off-resonance excitation. Under a bias of 0.5 V, the photodetector has a responsivity of ∼125 mA W^{-1} with a dark current lower than 20 nA thanks to the short BP channel. Relying on BP's high carrier mobility and the compact device structure, a high speed with a 3 dB bandwidth exceeding ∼1.42 GHz is obtained, which is limited by our instrument response. Our results indicate the BP photodetector integrated on a planar photonic crystal cavity has potential for constructing a compact on-chip photodetector of photonic integrated circuits.

KEYWORDS: *black phosphorus, photonic crystal cavity, photodetector, 2D materials, silicon photonics*

In the past decade, two-dimensional (2D) materials have been a focus of research to develop high-performance photodetectors relying on their merits of strong optical response, absence of dangling bonds, tunable electronic properties, etc.[1−9] Among them, few-layer black phosphorus (BP) is one of the most attractive 2D materials. Its direct bandgap with a small value of ∼0.3 eV promises the photodetection in the infrared spectral range.[10−12] A variety of BP photodetectors operating at the wavelengths of 1.5,[13] 2,[14] 3,[15] and 3.68−4.03 μm[16,17] have been reported. Superior to the infrared photodetectors based on semimetal 2D materials, such as graphene and WTe_2, BP phototransistors could have a high on/off ratio for suppressing dark current.[6,18−20] In addition, few-layer BP has high carrier mobilities and a strong anisotropic nature,[6,21] allowing a fast photoresponse and high gain in the armchair direction. For example, the photoresponsivity of tens to hundreds of mA W^{-1} from the near- to mid-infrared wavelengths and GHz operation in the BP devices were demonstrated.[13,14,16,22−24]

Unfortunately, 2D BP flakes only have a few atomic layers, hindering the effective light−matter coupling in BP photodetectors. For normal incident light, it is absorbed by the BP flake insufficiently since it only transmits across a few layers of BP atoms. This limits the photoresponsivity of BP photodetectors. To improve optical absorption in BP flakes, a promising strategy is integrating them with optical waveguides to extend the light−BP interaction length.[13,14,16,17,25] However, to ensure sufficiently high optical absorption, the channel length of the BP photodetector on the waveguide should be large enough, which inevitably induces a large device footprint, large dark current, and low operation speed.

Here, we report a BP photodetector integrated on a silicon planar photonic crystal (PPC) cavity. The PPC cavity could circulate light for a long time to strengthen the light−matter

Received: August 2, 2021

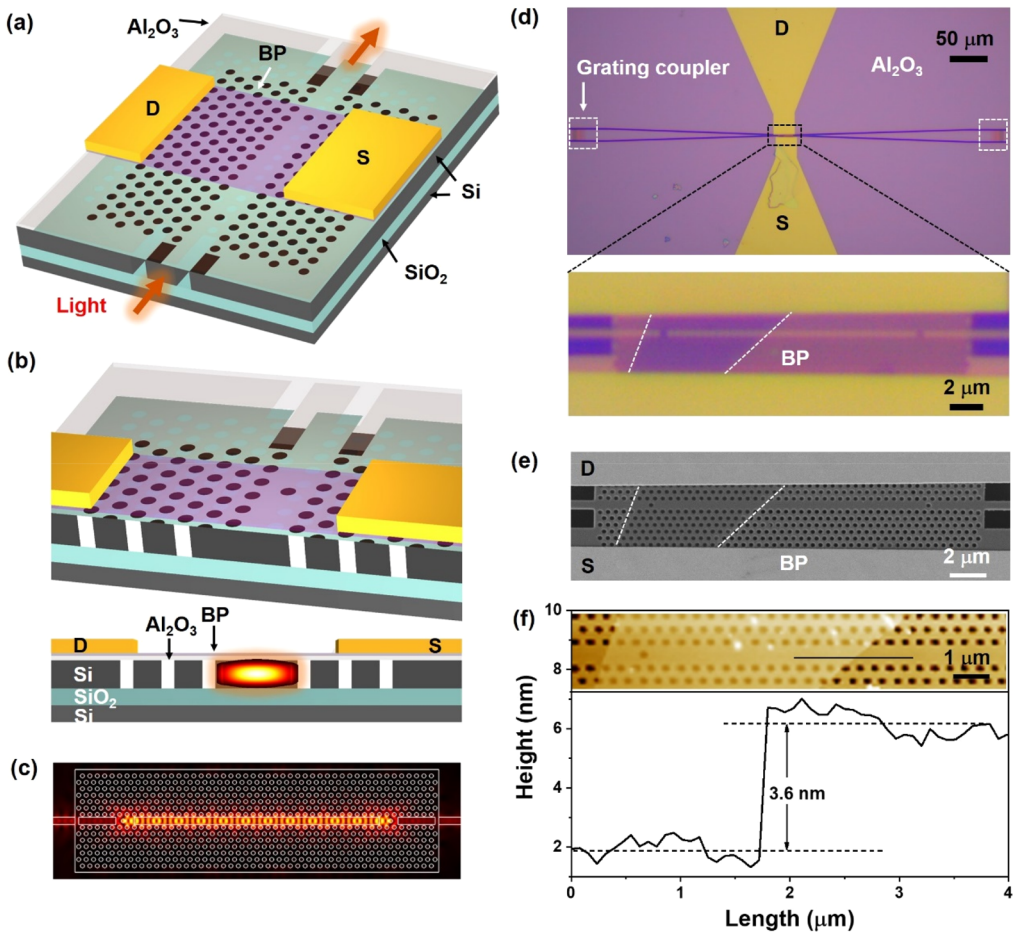

Figure 1. Design and fabricated device of the BP photodetector integrated on a PPC cavity. (a, b) Schematic diagrams of the PPC cavity-integrated BP photodetector, where D and S represent the drain and source electrodes. (c) Simulated energy distribution of the on-resonance mode in the PPC cavity. (d) Optical microscope images of the fabricated device. Top: Whole device with the tapered waveguides and grating couplers; Bottom: Zoomed-in region of the BP flake (indicated by the white dashed lines) coating on the PPC cavity. (e) Scanning electron microscopy (SEM) image of the fabricated device with the BP flake indicated by the white dashed line. (f) Top: Atomic force microscopy (AFM) image of a BP layer covering the PPC cavity. Bottom: AFM height profile marked by the black line in the top panel.

interaction in the integrated BP flake, which relieves the requirement of a long BP channel. Consequently, compared with the BP photodetectors integrated on optical waveguides, the PPC cavity-integrated configuration has a more compact footprint, which could simultaneously reduce the dark current and improve the response speed. With an on-resonance excitation, the responsivity is enhanced by 36 times with respect to that obtained with off-resonance excitation, which is the highest enhancement factor in the reported cavity-enhanced 2D material photodetectors. Under a bias of 0.5 V, the high responsivity of ~125 mA W^{-1} is obtained with a dark current lower than 20 nA. Also, a bandwidth of ~1.42 GHz is obtained in the impulse measurement, which is limited by our measurement instruments. In addition, the planar structure of the PPC cavity is compatible with the 2D geometry of the BP flake, facilitating its integration and construction of the photodetector. Our work might provide a new avenue to develop a compact integrated photodetector with high responsivity, low dark current, and fast dynamic response.

RESULTS AND DISCUSSION

Design and Fabrication of the PPC Cavity-Integrated BP Photodetector. Figure 1a,b schematically show the layout of the BP photodetector integrated on a PPC cavity. The employed PPC cavity is fabricated in a 220 nm thick silicon slab on a standard silicon-on-insulator (SOI) substrate with the techniques of electron beam lithography and inductively coupled plasmon etching. The buried oxide layer of the SOI has a thickness of 3 μm. The PPC cavity is formed by inserting two air holes in the PPC waveguide, which function as two mirrors to reflect the waveguiding mode. Before the integration of the BP flake, a process of atomic layer deposition is carried out to grow a 40 nm Al_2O_3 film over the silicon slab. Considering the employed silicon slab is lightly p-doped, this Al_2O_3 dielectric layer could electrically isolate the electrodes of the BP photodetector from the silicon slab. The BP flake is mechanically exfoliated from a bulk crystal and dry-transferred onto the PPC cavity with a polydimethylsiloxane (PDMS)-assisted technique.[26] To optimize the optical absorption efficiency and the channel carrier mobility of the BP flake, it is transferred with its armchair direction aligned with the carrier flow direction of the BP channel. The orientation angle of the BP flake is determined by measuring the polarization-dependent Raman spectra (see the Supporting Information). The result shows that the armchair direction of the transferred BP flake is close to the direction of the carrier flow in the channel based on the relative ratio of the B^2_g peak to the A^2_g peak, as depicted in Figure S1. Two metal electrodes (drain

https://doi.org/10.1021/acsphotonics.1c01168
ACS Photonics XXXX, XXX, XXX−XXX

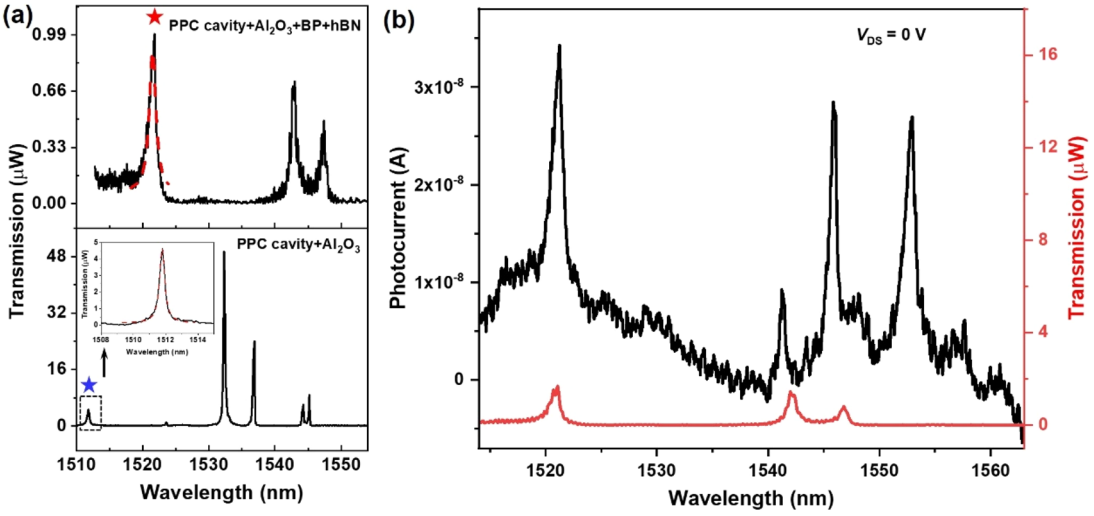

Figure 2. Enhanced photodetection in the device. (a) Transmission spectra of the PPC cavity measured before and after the integration of 2D materials. Spectra have been vertically translated for clarity. (b) Photocurrent spectra (left axis) of the BP photodetector measured within a wavelength range from 1500 to 1560 nm at zero bias, where the transmission spectrum (right axis) of the finished device is also superimposed for comparison.

and source) of the photodetectors are deposited on both sides of the BP flake with a mechanical transfer process.[27,28] As schematically shown in Figure 1b, the coated BP layer couples with the evanescent field of the PPC cavity. With the two air holes as the mirrors, the guiding mode would propagate in the waveguide backward and forward several times to interact with the BP flake, resulting in enhanced optical absorption. The resonance mode of the PPC cavity is simulated and shown in Figure 1c. The optical field is well localized between the two air holes, allowing the effective light−matter coupling in the top-coated BP flake.

Figure 1d displays optical microscope images of a fabricated device. Figure 1e,f show the corresponding scanning electron microscope (SEM) and atomic force microscope (AFM) images, showing the thickness of the BP layer of 3.6 nm. The PPC lattice is designed with an air-hole diameter of 240 nm and a lattice constant of 420 nm to support the photonic bandgap in the telecom-band spectral range. The PPC waveguide is formed by missing one line of air holes. The inserted two air holes in the waveguide have a distance about 15 μm. To facilitate the light coupling from optical fibers to the PPC waveguide and cavity, two grating couplers are designed at the two ends of the waveguide. The transferred BP layer has a length of ~7 μm over the PPC cavity, as shown in the bottom zoomed-in image of Figure 1d. After the deposition of the drain and source electrodes, a hexagonal boron nitride (h-BN) layer is finally transferred onto the device to encapsulate the BP and protect it from the degradation in ambient conditions. Note, the drain electrode has a separation of three rows of air holes from the central waveguide, as indicated by the SEM image of Figure 1e. According to the resonant mode shown in Figure 1c, the boundary of this drain electrode would interact with the resonant mode of the PPC cavity. At the same time, the electrical contact at this boundary would form a Schottky barrier, which provides an internal electric field over the BP region close to the electrode boundary. Hence, even if there is no external electrical bias, the photocarriers generated in the BP region around this electrode would be separated to yield a photocurrent, which enables a self-driven photodetection. Of course, an external bias could further facilitate the photocarrier separation to assist the photocurrent generation. To release the air bubbles between the 2D materials and metal electrodes and ensure their atomic level contact, the finished device is finally annealed in a vacuum environment.

Enhanced Photodetection in a PPC Cavity-Integrated BP Photodetector. The fabricated PPC cavity is optically characterized by measuring its transmission spectra, which could also present the optical absorption by the BP layer. By coupling a wavelength-tunable narrowband laser (1500 to 1630 nm) into one of the grating couplers and monitoring the output power at the other grating coupler using a power meter, the transmission spectra are obtained by sweeping the laser wavelengths. Before and after the integration of 2D materials, the transmission spectra of the PPC cavity are measured, as shown in Figure 2a. Multiple resonance peaks within a wavelength range between 1500 and 1560 nm are observed. The transfer of 2D materials and metal electrodes subsequently red-shift all the resonance peaks due to the changes of the dielectric environment around the cavity. As expected from the material absorption, the resonant peaks are lowered and broadened, manifesting the gradually reduced quality (Q) factors of the resonance peaks. Specifically, the resonance peak marked by the blue asterisk at the center wavelength of 1511.78 nm has a Q factor of 3860 ($Q1$), as estimated by fitting it to a Lorentz line shape, as shown in the inset of Figure 2a. After the transfer of 2D materials and metal electrodes, the resonance peak at 1511.78 nm is red-shifted to 1521.48 nm (the red asterisk) and the Q factor drops to 1260 ($Q2$).

From the transmission spectra shown in Figure 2a, it is possible to precisely extract the optical absorption by the BP flake integrated on the PPC cavity, which is assisted by a transfer matrix method.[29] The schematic model of the coupled BP-PPC cavity system is shown in Figure S3 of the Supporting Information. We assume the excitation mode (mode 1) a_1 and collection mode (mode 2) a_2 of the fiber−cavity coupling system. Due to the symmetric confinements of the two air-hole-enabled mirrors, the resonant mode of the PPC cavity decays equally into the forward and backward propagation modes. The steady-state solution to the transfer matrix

https://doi.org/10.1021/acsphotonics.1c01168
ACS Photonics XXXX, XXX, XXX−XXX

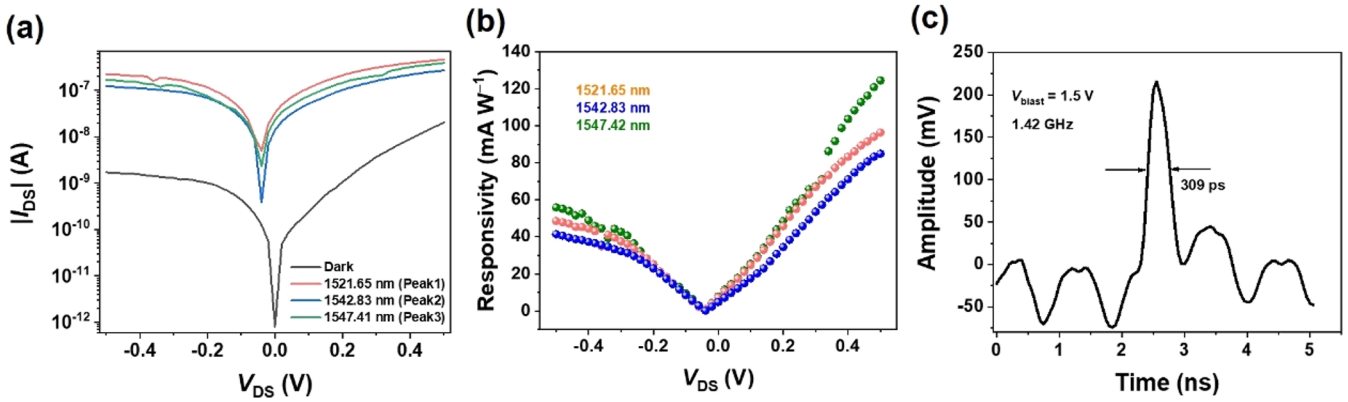

Figure 3. Steady and dynamic photoresponses of the BP photodetector integrated on a PPC cavity. (a) Measured current−voltage (I_{DS}−V_{DS}) characteristics of the BP photodetector without light illumination and with light incidence at three resonance wavelengths. (b) Photoresponsivity as functions of the bias voltages with the incident light at resonance peaks. (c) Measured impulse response of the BP photodetector integrated on a PPC cavity.

equations (see Supporting Information) then yields normalized transmission $T(\lambda)$ and reflection $R(\lambda)$ coefficients of the BP-integrated PPC cavity

$$T(\lambda) = \left| \frac{t^2}{-r^2 a e^{i2\pi/\lambda(n_1L_1+n_2L_2)} + a^{-1}e^{-i2\pi/\lambda(n_1L_1+n_2L_2)}} \right|^2 \quad (1)$$

$$R(\lambda) = \left| -\frac{r a e^{i2\pi/\lambda(n_1L_1+n_2L_2)} - r a^{-1}e^{-i2\pi/\lambda(n_1L_1+n_2L_2)}}{-r^2 a e^{i2\pi/\lambda(n_1L_1+n_2L_2)} + a^{-1}e^{-i2\pi/\lambda(n_1L_1+n_2L_2)}} \right|^2 \quad (2)$$

where r and t denote the amplitude reflection and transmission coefficients. BP induces additional cavity loss parameter $a = \exp(-i2\pi k L_2/\lambda)$. L_2 and $L_1 + L_2$ are the length of the BP flake and the distance of the two air holes, respectively. n_1 and n_2 are effective refractive indices for the BP-integrated cavity and bare cavity, respectively. λ is the operation wavelength. Note that for the experimental conditions with fiber coupled with the cavity, the measured signal corresponds to what we designate above as transmission. With $Q1$ and $Q2$ obtained from above, we extract that $r_1 = 0.9685$ and $k_1 = 0.0019$ according to eqs 1 and 2 in the transfer matrix model[29,30] for the resonance peak marked by the asterisks in Figure 2a. With the obtained parameters r_1 and k_1, we also plot the normalized transmission, reflection, and absorption spectra (see Figure S4 in the Supporting Information). We employ the ratio of $A(\lambda)$ and $T(\lambda)$ to eliminate the effect of the grating coupling efficiency and then obtain the absorption power by the BP flake. The absorption power $P_{absorption}$ is determined by $P_{transmission} \times A(\lambda)/T(\lambda)$ (see Figure S5 in the Supporting Information). Using the same approach, we extract the parameters r, k, and $A(\lambda)/T(\lambda)$ of the other resonance peaks in the measured transmission spectra (shown in Figure 2a) and plot the normalized transmission, absorption, and reflection spectra in Figure S4 of the Supporting Information.

The photoresponse of the PPC cavity-integrated BP photodetector is then characterized with the assistance of a highly sensitive electrical source meter. As discussed above, since the drain electrode could provide an internal electric field over the BP channel to couple with the resonant mode, the fabricated device could operate as a self-driven photodetector. Hence, without the application of an electrical bias, by coupling the laser into the device, photocurrents are obtained between the drain and source electrodes. We measured the photocurrent spectra by sweeping the incident wavelength from 1510 to 1550 nm at a fixed laser power. As displayed in Figure 2b, the zero-bias photocurrents show multiple peaks, which overlap with the resonant peaks observed in the transmission spectra of the BP-integrated PPC cavity. It implies the improved photodetection enhanced by the cavity modes. As discussed above, the localized resonance modes of the PPC cavity could support effective light−matter interaction in the integrated BP flake, which therefore generates considerable photocarriers. With the built-in electric field by the metal electrodes, photocurrents are generated across the BP channel. Comparing the photocurrents obtained when the incident light is on- and off-resonance, we obtain an enhancement factor of 36-fold by the resonance mode at the wavelength of 1547.42 nm. There are several works also reported on cavity-enhanced 2D material photodetectors. Here, the cavity-enhancement factor obtained from the fabricated BP photodetector is superior to the previous reports.[31−33] With an on-resonance optical excitation, the photoresponsivity is calculated as 7.8 mA/W under the zero-bias condition.

Steady and Dynamic Photoresponses of the PPC Cavity-Integrated BP Photodetector. To further improve the responsivity of the BP photodetector at the low dark current level, we apply a small bias voltage V_{DS} to strengthen the separation of the photogenerated carriers in the channel. Current−voltage (I_{DS}−V_{DS}) curves are recorded without light illumination and with light incidence at the three resonance wavelengths, as shown in Figure 3a. Without optical excitation, the device has a very tiny dark current. Even with a bias voltage of 0.5 V, the dark current is still lower than 20 nA. On the contrary, a pronounced photoresponse is observed when light is coupled into the PPC cavity. Asymmetric currents under positive and negative bias conditions are induced by the asymmetric contacting scheme. The responsivity is extracted as the ratio of the photocurrent and the BP optical absorption power. It increases with the applied bias voltage that assists the extraction of photocarriers. Increasing the applied bias to a moderately high value of 0.5 V, as shown in Figure 3b, it yields responsivities of 96, 84, and 125 mA W^{-1} at the resonance wavelengths of 1521.65, 1542.83, and 1547.42 nm, respectively. The internal quantum efficiency (IQE), η_{IQE}, achieves 10% at the resonance wavelength of 1547.42 nm ($\eta_{IQE} = R \times$

https://doi.org/10.1021/acsphotonics.1c01168
ACS Photonics XXXX, XXX, XXX−XXX

$\hbar\omega/q$), where R, $\hbar$, ω, and q are the responsivity, reduced Planck constant, light angular frequency, and the elementary charge, respectively. The different responsivities at the three resonance wavelengths are attributed to the different coupling strengths between BP and resonance modes of the PPC cavity. We intentionally keep the bias voltage low in the steady-state photodetection measurements so as not to damage the devices. In fact, the photocurrent and the IQE are expected to further increase for larger applied bias voltages, limited only by break down and saturation of absorption.

Under a small bias voltage condition, the idea utilized for improving the responsivity of the device also includes leveraging a thicker BP layer or applying a gate electric field. We also make another device with the thicker BP flake and the gate modulation, which achieves a responsivity of 639 mA W^{-1} at the small bias of −0.2 V under the gate voltage of −2 V with a BP thickness of 7.9 nm (see Figures S6, S7, S8, and S9 in the Supporting Information).

To evaluate the dynamic response of the PPC cavity-integrated BP photodetector, we implement an impulse response measurement. A picosecond pulsed laser at the wavelength of 1550 nm is employed as the incident light source, which provides a train of 5 ps long (full width at half-maximum) optical pulses. By coupling the optical pulses into the device, the generated electrical pulses are monitored with an oscilloscope (see Figure S10 in the Supporting Information). Figure 3c displays the measured impulse responses of the device, from which we extract a pulse duration of the photocurrent at a full-width at half-maximum (fwhm) of $\Delta t \approx 309$ ps. The electrical bandwidth can then be derived using the time-bandwidth product. Assuming a Gaussian impulse response, $f_{3\,\mathrm{dB}} \approx 0.44/\Delta t \approx 1.42$ GHz is obtained, which is the limit of our measurement setup. The RC constant and transit time of our device are also discussed in the Supporting Information, which are not the limiting factors of the obtained 1.42 GHz response speed. We anticipate that the device might work at even higher frequencies.

CONCLUSIONS

In conclusion, we have demonstrated a high-performance BP photodetector integrated on a PPC cavity. Improved by the enhanced light−matter interaction in the PPC cavity, the optical absorption in the integrated BP flake is strengthened significantly. It therefore allows us to shrink the length of the BP channel of the photodetector. A device with a 7 μm BP length is fabricated. The photoresponsivity is enhanced by 36-fold for the on-resonance light illumination, which is superior to the previous reports about cavity-enhanced 2D material photodetectors. A high responsivity of 125 mA W^{-1} under 0.5 V bias is obtained, which has a dark current lower than 20 nA and a 3 dB cutoff frequency exceeding 1.42 GHz. While the temperature stability measurements are not carried out on our fabricated device, the previously reported work showed that the BP photodetector is not sensitive to the environmental temperature.[14] Combined with the recent development of large-scale growth of few-layer BP on silicon,[34,35] the demonstrated PPC cavity-integrated BP photodetector with the feasibility of efficient and ultracompact photodetection is expected to be commercialized in future photonic integrated circuits.[36]

ASSOCIATED CONTENT

Supporting Information

The Supporting Information is available free of charge at https://pubs.acs.org/doi/10.1021/acsphotonics.1c01168.

Raman characterization; design of the PPC cavity; model analysis for the coupled system of BP-PPC cavity; another PPC cavity-integrated BP photodetector; impulse response measurement for the device; comparison with prior-art 2D material photodetectors integrated on silicon waveguides or microcavities (PDF)

AUTHOR INFORMATION

Corresponding Author

Xuetao Gan − *Key Laboratory of Light Field Manipulation and Information Acquisition, Ministry of Industry and Information Technology, and Shaanxi Key Laboratory of Optical Information Technology, School of Physical Science and Technology, Northwestern Polytechnical University, 710129 Xi'an, China;* orcid.org/0000-0003-2469-5807; Email: xuetaogan@nwpu.edu.cn

Authors

Ruijuan Tian − *Key Laboratory of Light Field Manipulation and Information Acquisition, Ministry of Industry and Information Technology, and Shaanxi Key Laboratory of Optical Information Technology, School of Physical Science and Technology, Northwestern Polytechnical University, 710129 Xi'an, China*

Linpeng Gu − *Key Laboratory of Light Field Manipulation and Information Acquisition, Ministry of Industry and Information Technology, and Shaanxi Key Laboratory of Optical Information Technology, School of Physical Science and Technology, Northwestern Polytechnical University, 710129 Xi'an, China*

Yingke Ji − *Key Laboratory of Light Field Manipulation and Information Acquisition, Ministry of Industry and Information Technology, and Shaanxi Key Laboratory of Optical Information Technology, School of Physical Science and Technology, Northwestern Polytechnical University, 710129 Xi'an, China*

Chen Li − *Key Laboratory of Light Field Manipulation and Information Acquisition, Ministry of Industry and Information Technology, and Shaanxi Key Laboratory of Optical Information Technology, School of Physical Science and Technology, Northwestern Polytechnical University, 710129 Xi'an, China*

Yuxin Chen − *Key Laboratory of Light Field Manipulation and Information Acquisition, Ministry of Industry and Information Technology, and Shaanxi Key Laboratory of Optical Information Technology, School of Physical Science and Technology, Northwestern Polytechnical University, 710129 Xi'an, China*

Siqi Hu − *Key Laboratory of Light Field Manipulation and Information Acquisition, Ministry of Industry and Information Technology, and Shaanxi Key Laboratory of Optical Information Technology, School of Physical Science and Technology, Northwestern Polytechnical University, 710129 Xi'an, China*

Zhiwen Li − *Key Laboratory of Light Field Manipulation and Information Acquisition, Ministry of Industry and Information Technology, and Shaanxi Key Laboratory of Optical Information Technology, School of Physical Science*

and Technology, Northwestern Polytechnical University, 710129 Xi'an, China

Jianlin Zhao − *Key Laboratory of Light Field Manipulation and Information Acquisition, Ministry of Industry and Information Technology, and Shaanxi Key Laboratory of Optical Information Technology, School of Physical Science and Technology, Northwestern Polytechnical University, 710129 Xi'an, China*

Complete contact information is available at: https://pubs.acs.org/10.1021/acsphotonics.1c01168

Notes

The authors declare no competing financial interest.

■ ACKNOWLEDGMENTS

Financial support was provided by the Key Research and Development Program (Grant No. 2018YFA0307200), the National Natural Science Foundations of China (Grant Nos. 61775183, 11634010, and 61905196), the Key Research and Development Program in Shaanxi Province of China (Grant No. 2020JZ-10), and the Fundamental Research Funds for the Central Universities (Grant Nos. 3102019JC008, 3102018jcc034, and 310201911cx032). The authors thank the Analytical & Testing Center of NPU for the assistance with device fabrication.

■ REFERENCES

(1) Gan, X.; Shiue, R. J.; Gao, Y.; Meric, I.; Heinz, T. F.; Shepard, K.; Hone, J.; Assefa, S.; Englund, D. Chip-Integrated Ultrafast Graphene Photodetector with High Responsivity. *Nat. Photonics* **2013**, *7* (11), 883−887.

(2) Xia, F.; Wang, H.; Xiao, D.; Dubey, M.; Ramasubramaniam, A. Two-Dimensional Material Nanophotonics. *Nat. Photonics* **2014**, *8* (12), 899−907.

(3) Pospischil, A.; Humer, M.; Furchi, M. M.; Bachmann, D.; Guider, R.; Fromherz, T.; Mueller, T. CMOS-Compatible Graphene Photodetector Covering All Optical Communication Bands. *Nat. Photonics* **2013**, *7* (11), 892−896.

(4) Lopez-Sanchez, O.; Lembke, D.; Kayci, M.; Radenovic, A.; Kis, A. Ultrasensitive Photodetectors Based on Monolayer MoS_2. *Nat. Nanotechnol.* **2013**, *8* (7), 497−501.

(5) Flöry, N.; Ma, P.; Salamin, Y.; Emboras, A.; Taniguchi, T.; Watanabe, K.; Leuthold, J.; Novotny, L. Waveguide-Integrated van Der Waals Heterostructure Photodetector at Telecom Wavelengths with High Speed and High Responsivity. *Nat. Nanotechnol.* **2020**, *15* (2), 118−124.

(6) Xia, F.; Wang, H.; Jia, Y. Rediscovering Black Phosphorus as an Anisotropic Layered Material for Optoelectronics and Electronics. *Nat. Commun.* **2014**, *5*, 4458.

(7) Gao, L.; Ma, C.; Wei, S.; Kuklin, A. V.; Zhang, H.; Ågren, H. Applications of Few-Layer Nb_2C MXene: Narrow-Band Photodetectors and Femtosecond Mode-Locked Fiber Lasers. *ACS Nano* **2021**, *15* (1), 954−965.

(8) Pei, J.; Yang, J.; Yildirim, T.; Zhang, H.; Lu, Y. Many-Body Complexes in 2D Semiconductors. *Adv. Mater.* **2019**, *31* (2), 1706945.

(9) Zhang, Y.; Huang, P.; Guo, J.; Shi, R.; Huang, W.; Shi, Z.; Wu, L.; Zhang, F.; Gao, L.; Li, C.; Zhang, X.; Xu, J.; Zhang, H. Graphdiyne-Based Flexible Photodetectors with High Responsivity and Detectivity. *Adv. Mater.* **2020**, *32* (23), 2001082.

(10) Xia, F.; Wang, H.; Hwang, J. C. M.; Neto, A. H. C.; Yang, L. Black Phosphorus and Its Isoelectronic Materials. *Nat. Rev. Phys.* **2019**, *1* (5), 306−317.

(11) Li, L.; Kim, J.; Jin, C.; Ye, G. J.; Qiu, D. Y.; da Jornada, F. H.; Shi, Z.; Chen, L.; Zhang, Z.; Yang, F.; Watanabe, K.; Taniguchi, T.; Ren, W.; Louie, S. G.; Chen, X. H.; Zhang, Y.; Wang, F. Direct Observation of the Layer-Dependent Electronic Structure in Phosphorene. *Nat. Nanotechnol.* **2017**, *12* (1), 21−25.

(12) Tian, R.; Fei, R.; Hu, S.; Li, T.; Zheng, B.; Shi, Y.; Zhao, J.; Zhang, L.; Gan, X.; Wang, X. Observation of Excitonic Series in Mono- and Few-Layer Black Phosphorus. *Phys. Rev. B: Condens. Matter Mater. Phys.* **2020**, *101*, 235407.

(13) Youngblood, N.; Chen, C.; Koester, S. J.; Li, M. Waveguide-Integrated Black Phosphorus Photodetector with High Responsivity and Low Dark Current. *Nat. Photonics* **2015**, *9* (4), 247−252.

(14) Yin, Y.; Cao, R.; Guo, J.; Liu, C.; Li, J.; Feng, X.; Wang, H.; Du, W.; Qadir, A.; Zhang, H.; Ma, Y.; Gao, S.; Xu, Y.; Shi, Y.; Tong, L.; Dai, D. High-Speed and High-Responsivity Hybrid Silicon/Black-Phosphorus Waveguide Photodetectors at 2 μm. *Laser Photonics Rev.* **2019**, *13* (6), 1900032.

(15) Yan, W.; Shresha, V. R.; Jeangros, Q.; Azar, N. S.; Balendhran, S.; Ballif, C.; Crozier, K.; Bullock, J. Spectrally Selective Mid-Wave Infrared Detection Using Fabry-Pérot Cavity Enhanced Black Phosphorus 2D Photodiodes. *ACS Nano* **2020**, *14* (10), 13645−13651.

(16) Huang, L.; Dong, B.; Guo, X.; Chang, Y.; Chen, N.; Huang, X.; Liao, W.; Zhu, C.; Wang, H.; Lee, C.; Ang, K.-W. Waveguide-Integrated Black Phosphorus Photodetector for Mid-Infrared Applications. *ACS Nano* **2019**, *13* (1), 913−921.

(17) Ma, Y.; Dong, B.; Wei, J.; Chang, Y.; Huang, L.; Ang, K.-W.; Lee, C. High-Responsivity Mid-Infrared Black Phosphorus Slow Light Waveguide Photodetector. *Adv. Opt. Mater.* **2020**, *8*, 2000337.

(18) Li, L.; Yu, Y.; Ye, G. J.; Ge, Q.; Ou, X.; Wu, H.; Feng, D.; Chen, X. H.; Zhang, Y. Black Phosphorus Field-Effect Transistors. *Nat. Nanotechnol.* **2014**, *9* (5), 372−377.

(19) Li, C.; Chen, C.; Chen, J.; He, T.; Li, H.; Yang, Z.; Xie, L.; Wang, Z.; Zhang, K. High-Performance Junction Field-Effect Transistor Based on Black Phosphorus/β-Ga_2O_3 Heterostructure. *J. Semicond.* **2020**, *41* (8), 082002.

(20) Liu, H.; Neal, A. T.; Zhu, Z.; Luo, Z.; Xu, X.; Tománek, D.; Ye, P. D. Phosphorene: An Unexplored 2D Semiconductor with a High Hole Mobility. *ACS Nano* **2014**, *8* (4), 4033−4041.

(21) Qiao, J.; Kong, X.; Hu, Z. X.; Yang, F.; Ji, W. High-Mobility Transport Anisotropy and Linear Dichroism in Few-Layer Black Phosphorus. *Nat. Commun.* **2014**, *5*, 4475.

(22) Buscema, M.; Groenendijk, D. J.; Blanter, S. I.; Steele, G. A.; Van Der Zant, H. S. J.; Castellanos-Gomez, A. Fast and Broadband Photoresponse of Few-Layer Black Phosphorus Field-Effect Transistors. *Nano Lett.* **2014**, *14* (6), 3347−3352.

(23) Wang, H.; Wang, X.; Xia, F.; Wang, L.; Jiang, H.; Xia, Q.; Chin, M. L.; Dubey, M.; Han, S. Black Phosphorus Radio-Frequency Transistors. *Nano Lett.* **2014**, *14* (11), 6424−6429.

(24) Yuan, H.; Liu, X.; Afshinmanesh, F.; Li, W.; Xu, G.; Sun, J.; Lian, B.; Curto, A. G.; Ye, G.; Hikita, Y.; Shen, Z.; Zhang, S. C.; Chen, X.; Brongersma, M.; Hwang, H. Y.; Cui, Y. Polarization-Sensitive Broadband Photodetector Using a Black Phosphorus Vertical p-n Junction. *Nat. Nanotechnol.* **2015**, *10* (8), 707−713.

(25) Wang, T.; Hu, S.; Chamlagain, B.; Hong, T.; Zhou, Z.; Weiss, S. M.; Xu, Y.-Q. Visualizing Light Scattering in Silicon Waveguides with Black Phosphorus Photodetectors. *Adv. Mater.* **2016**, *28* (33), 7162−7166.

(26) Castellanos-Gomez, A.; Buscema, M.; Molenaar, R.; Singh, V.; Janssen, L.; Van Der Zant, H. S. J.; Steele, G. A. Deterministic Transfer of Two-Dimensional Materials by All-Dry Viscoelastic Stamping. *2D Mater.* **2014**, *1* (1), 011002.

(27) Liu, Y.; Guo, J.; Zhu, E.; Liao, L.; Lee, S.-J.; Ding, M.; Shakir, I.; Gambin, V.; Huang, Y.; Duan, X. Approaching the Schottky−Mott Limit in van Der Waals Metal−Semiconductor Junctions. *Nature* **2018**, *557* (7707), 696−700.

(28) Went, C. M.; Wong, J.; Jahelka, P. R.; Kelzenberg, M.; Biswas, S.; Atwater, H. A. A New Metal Transfer Process for van Der Waals Contacts to Vertical Schottky-Junction Transition Metal Dichalcogenide Photovoltaics. *Sci. Adv.* **2019**, *5* (12), eaax6061.

(29) Fan, S. Sharp Asymmetric Line Shapes in Side-Coupled Waveguide-Cavity Systems. *Appl. Phys. Lett.* **2002**, *80*, 908.

(30) Quan, Q.; Deotare, P. B.; Loncar, M. Photonic Crystal Nanobeam Cavity Strongly Coupled to the Feeding Waveguide. *Appl. Phys. Lett.* **2010**, *96* (20), 203102.
(31) Shiue, R. J.; Gan, X.; Gao, Y.; Li, L.; Yao, X.; Szep, A.; Walker, D.; Hone, J.; Englund, D. Enhanced Photodetection in Graphene-Integrated Photonic Crystal Cavity. *Appl. Phys. Lett.* **2013**, *103* (24), 241109.
(32) Chen, X.; Wang, F.; Gu, Q.; Yang, J.; Yu, M.; Kwong, D.-l.; Wong, C. W.; Yang, H.; Zhou, H.; Zhou, S. Multifunctional Optoelectronic Device Based on Graphene-Coupled Silicon Photonic Crystal Cavities. *Opt. Express* **2021**, *29* (7), 11094−11105.
(33) Engel, M.; Steiner, M.; Lombardo, A.; Ferrari, A. C.; Lähneysen, H. V.; Avouris, P.; Krupke, R. Light-Matter Interaction in a Microcavity-Controlled Graphene Transistor. *Nat. Commun.* **2012**, *3* (5), 906.
(34) Xu, Y.; Shi, X.; Zhang, Y.; Zhang, H.; Zhang, Q.; Huang, Z.; Xu, X.; Guo, J.; Zhang, H.; Sun, L.; Zeng, Z.; Pan, A.; Zhang, K. Epitaxial Nucleation and Lateral Growth of High-Crystalline Black Phosphorus Films on Silicon. *Nat. Commun.* **2020**, *11* (1), 1330.
(35) Wu, Z.; Lyu, Y.; Zhang, Y.; Ding, R.; Zheng, B.; Yang, Z.; Lau, S. P.; Chen, X. H.; Hao, J. Large-Scale Growth of Few-Layer Two-Dimensional Black Phosphorus. *Nat. Mater.* **2021**, *20*, 1203−1209.
(36) Liang, D.; E. Bowers, J. Recent Progress in Heterogeneous III-V-on-Silicon Photonic Integration. *Light Adv. Manuf.* **2021**, *2* (1), 59−83.

https://doi.org/10.1021/acsphotonics.1c01168
ACS Photonics XXXX, XXX, XXX−XXX